Research Article | Vol. 26, No. 14 | 9 Jul 2018 | OPTICS EXPRESS 18302
Optics EXPRESS

1.3 μm InAs/GaAs quantum dot DFB laser integrated on a Si waveguide circuit by means of adhesive die-to-wafer bonding

SARAH UVIN,[1,2,*] SULAKSHNA KUMARI,[1,2] ANDREAS DE GROOTE,[1,2] STEVEN VERSTUYFT,[1,2] GUY LEPAGE,[3] PETER VERHEYEN,[3] JORIS VAN CAMPENHOUT,[3] GEERT MORTHIER,[1,2] DRIES VAN THOURHOUT,[1,2] AND GUNTHER ROELKENS[1,2]

[1] *Photonics Research Group, Department of Information Technology, Ghent University - imec, iGent, Technologiepark-Zwijnaarde 15, 9052 Ghent, Belgium*
[2] *Center for Nano- and Biophotonics (NB-Photonics), Ghent University, Ghent, Belgium*
[3] *imec, Kapeldreef 75, 3001 Leuven, Belgium*
[*] *sarah.uvin@ugent.be*

Abstract: In this paper we report a single mode InAs/GaAs quantum dot distributed feedback laser at 1.3 μm wavelength heterogeneously integrated on a Si photonics waveguide circuit. Single mode lasing around 1300 nm with a side-mode suppression ratio higher than 40 dB is demonstrated. High temperature operation with continuous wave lasing up to 100°C is obtained. Threshold current densities as low as 205 A/cm^2 were measured. These devices are attractive candidates to use in uncooled silicon photonic transceivers in data centers.

OCIS codes: (250.5300) Photonic integrated circuits; (250.5590) Quantum-well, -wire and -dot devices; (250.5960) Semiconductor lasers; (140.3490) Lasers, distributed-feedback.

References and links

1. D. A. Miller, "Rationale and challenges for optical interconnects to electronic chips," Proc. IEEE **88**, 728–749 (2000).
2. Z. Zhou, B. Yin and J. Michel, "On-chip light sources for silicon photonics," Light. Sci. Appl. **4**, e358 (2015).
3. M. Sugawara and M. Usami, "Quantum dot devices: Handling the heat," Nat. Photonics **3**, 30–31 (2009).
4. H. Liu, D. Childs, T. Badcock, K. Groom, I. Sellers, M. Hopkinson, R. Hogg, D. Robbins, D. Mowbray and M. Skolnick, "High-performance three-layer 1.3-μm InAs-GaAs quantum-dot lasers with very low continuous-wave room-temperature threshold currents," IEEE Photon. Technol. Lett. **17**, 1139–1141 (2005).
5. D. Liang, G. Kurczveil, X. Huang, C. Zhang, S. Srinivasan, Z. Huang, M. A. Seyedi, K. Norris, M. Fiorentino, J. E. Bowers and R. G. Beausoleil, "Heterogeneous silicon light sources for datacom applications," Opt. Fiber Technol., in press (2017).
6. D. Jung, Z. Zhang, J. Norman, R. Herrick, M. Kennedy, P. Patel, K. Turnlund, C. Jan, Y. Wan, A. Gossard and J. Bowers, "Highly reliable low threshold InAs quantum dot lasers on on-axis (001) Si with 87% injection efficiency," ACS Photonics **5**, 1094–1100 (2018).
7. S. Chen, W. Li, J. Wu, Q. Jiang, M. Tang, S. Shutts, S. N. Elliott, A. Sobiesierski, A. J. Seeds, I. Ross, P. Smowton and H. Liu, "Electrically pumped continuous-wave III–V quantum dot lasers on silicon," Nat. Photonics **10**, 307 (2016).
8. N. Hatori, Y. Urino, T. Shimizu, M. Okano, T. Yamamoto, M. Mori, T. Nakamura and Y. Arakawa, "Quantum dot laser for a light source of an athermal silicon optical interposer," Photonics **2**, 355–364 (2015).
9. K. Tanabe, K. Watanabe and Y. Arakawa, "Iii-v/si hybrid photonic devices by direct fusion bonding," Sci. Rep. **2**, 349 (2012).
10. Y.-H. Jhang, K. Tanabe, S. Iwamoto and Y. Arakawa, "Inas/gaas quantum dot lasers on silicon-on-insulator substrates by metal-stripe wafer bonding," IEEE Photon. Technol. Lett. **27**, 875–878 (2015).
11. G. Kurczveil, D. Liang, M. Fiorentino and R. G. Beausoleil, "Robust hybrid quantum dot laser for integrated silicon photonics," Opt. Express **24**, 16167–16174 (2016).
12. B. Jang, K. Tanabe, S. Kako, S. Iwamoto, T. Tsuchizawa, H. Nishi, N. Hatori, M. Noguchi, T. Nakamura, K. Takemasa, M. Sugawara and Y. Arakawa, "A hybrid silicon evanescent quantum dot laser," Appl. Phys. Express **9**, 092102 (2016).
13. A. W. Fang, E. Lively, Y.-H. Kuo, D. Liang and J. E. Bowers, "A distributed feedback silicon evanescent laser," Opt. Express **16**, 4413–4419 (2008).
14. S. Keyvaninia, S. Verstuyft, L. Van Landschoot, F. Lelarge, G.-H. Duan, S. Messaoudene, J.-M. Fedeli, T. D. Vries, B. Smalbrugge, E. J. Geluk, J. Bolk, M. Smit, G. Morthier, D. Van Thourhout and G. Roelkens, "Heterogeneously

#325323 https://doi.org/10.1364/OE.26.018302
Journal © 2018 Received 6 Mar 2018; revised 16 May 2018; accepted 11 Jun 2018; published 2 Jul 2018

Optics EXPRESS

integrated iii-v/silicon distributed feedback lasers," Opt. Lett. **38**, 5434–5437 (2013).
15. N. Anscombe, "Join up the quantum dots," Nat. Photonics **1**, 360–361 (2007).
16. S. Keyvaninia, M. Muneeb, S. Stankovic, P. Van Veldhoven, D. Van Thourhout and G. Roelkens, "Ultra-thin dvs-bcb adhesive bonding of iii-v wafers, dies and multiple dies to a patterned silicon-on-insulator substrate," Opt. Mater. Express **3**, 35–46 (2013).
17. E. P. Haglund, S. Kumari, P. Westbergh, J. S. Gustavsson, G. Roelkens, R. Baets and A. Larsson, "Silicon-integrated short-wavelength hybrid-cavity vcsel," Opt. Express **23**, 33634–33640 (2015).
18. D. Vermeulen, Y. De Koninck, Y. Li, E. Lambert, W. Bogaerts, R. Baets and G. Roelkens, "Reflectionless grating couplers for silicon-on-insulator photonic integrated circuits," Opt. Express **20**, 22278–22283 (2012).
19. C. Zhang, S. Srinivasan, Y. Tang, M. J. Heck, M. L. Davenport, and J. E. Bowers, "Low threshold and high speed short cavity distributed feedback hybrid silicon lasers," Opt. Express **22**, 10202–10209 (2014).
20. Q. Li, X. Wang, H. Chen, Y. Huang, C. Hou, J. Wang, R. Zhang, J. Ning, J. Min and C. Zheng, "Development of modulation p-doped 1310 nm inas/gaas quantum dot laser materials, and ultra-short cavity fabry-perot and distributed-feedback laser diodes," ACS Photonics **5**, 1084–1093 (2018).

1. Introduction

In the present Big Data era, the demand for higher bandwidths is increasing at an unprecedented pace. This trend requires high-performance interconnects that can sustain this high bandwidth without consuming exorbitant amounts of energy. Silicon photonics is emerging as an important platform for the realization of power-efficient, high-speed optical transceivers [1]. However, currently the lack of cost-effective integration of the light source limits silicon-based photonic integrated circuits (PIC) deployment in these fields. In order to become a competitive technology, on-chip lasers operating at high ambient temperature and with low-loss coupling to the silicon waveguide circuits are very important [2].

Due to the three dimensional confinement of carriers, InAs/GaAs quantum dot (QD) lasers inherently have a more stable performance over the 20°C-100°C temperature range compared to quantum well lasers [3]. Furthermore, they can achieve very low threshold current densities [4] and because of the way QDs are grown they have a wider gain spectrum compared to conventional quantum well lasers making this material system an excellent candidate for creating multi-wavelength transmitters.

The integration of QD lasers directly on the silicon photonics platform, leveraging the well-developed CMOS fabrication infrastructure and its economies of scale, can provide a distinct cost advantage over other optical technologies. At the same time it would reduce coupling losses and packaging costs inherent in multi-chip solutions. Furthermore, the integration of the laser source directly on silicon enables the scaling of the aggregate bandwidth of transceivers to the Terabit/s range. [5]

There are multiple ways to integrate lasers with silicon photonic circuits. Typical integration schemes include hetero-epitaxy of III-V materials [6, 7], flip-chip bonding [8] and wafer bonding [9]. Many wafer-bonding approaches use a metal layer between the silicon and the GaAs wafers to facilitate bonding [10], which complicates the coupling to an underlying silicon waveguide circuit. Wafer-bonded QD lasers without a metal layer have recently been demonstrated [11,12]. Since both electrical contacts are now laterally formed on the III-V, low-loss coupling of the laser light to a silicon waveguide is possible. This allows for the integration of heterogeneous III-V-on-Si quantum dot lasers with high-quality Si photonic components.

Distributed-feedback (DFB) lasers are important optical sources, providing longitudinal single-mode emission with a relatively narrow line width. They are essential for wavelength division multiplexing (WDM) systems [13, 14]. In this paper we report the first single mode InAs/GaAs quantum dot DFB lasers on a silicon substrate with coupling to a silicon waveguide. Continuous wave (CW) laser operation up to 100°C is shown. The DFB laser structures demonstrated in this paper are based on second order gratings defined in the silicon circuit with Bragg wavelengths around 1300 nm and 1320 nm.

Optics EXPRESS

2. Device design and fabrication

The three-dimensional layout of the DFB laser is shown in Fig. 1(a). The laser cavity consists of a DFB grating defined in the silicon waveguide layer with the III-V gain region bonded on top. Multiple devices with different grating periods and thus lasing wavelengths were fabricated in parallel. The lasers discussed here have second order DFB gratings with a phase-shift in the middle with grating periods of 392 nm and 400 nm, which corresponds with Bragg wavelengths of 1300 nm and 1320 nm, respectively. Due to fabrication limitations, we opted for a second order grating with a duty cycle of 70%. The grating κ is estimated to be around 77 cm^{-1} for both grating periods. The III-V gain section is 800 μm (period: 392 nm) and 1000 μm (period: 400 nm) long (not including the 215 μm-long spotsize converters on each side). A 215 μm-long tapered spotsize converter is used to couple the light from the gain section into the passive silicon waveguides. The III-V taper is a piecewise linear taper that quickly tapers (L = 35 μm) from a 3.7 μm mesa width to an 1.7 μm wide waveguide width after which a slower adiabatic taper (L = 180 μm) is implemented by tapering both the III-V and silicon waveguide structure.

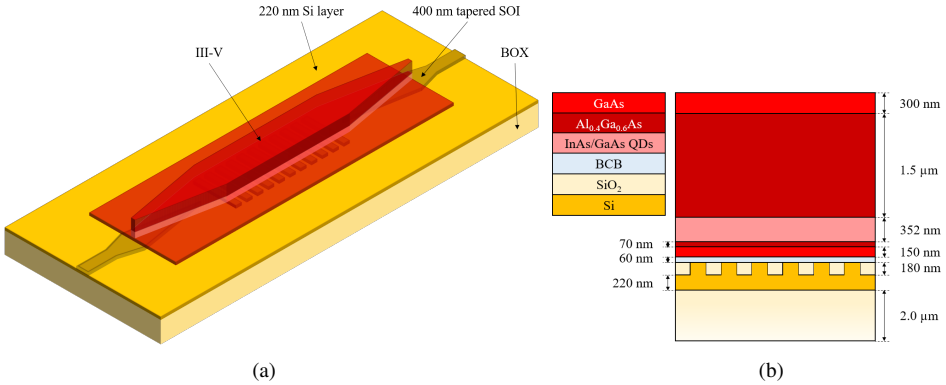

Fig. 1. III-V/Si distributed feedback laser design: (a) 3D view of the III-V-on-silicon DFB laser; (b) cross-sectional diagram of the laser structure.

A schematic cross-section of the III-V-on-silicon waveguide structure is depicted in Fig. 1(b). The laser consists of a planarized SOI wafer containing the silicon waveguides and gratings defined in a 400 nm thick silicon waveguide layer using 193 nm deep UV lithography (180 nm etch depth) fabricated in a CMOS pilot-line at imec. The GaAs quantum dot epitaxial layer stack is adhesively bonded to the planarized silicon-on-insulator (SOI) using a 60 nm-thick divinylsiloxane-bisbenzocyclobutene (DVS-BCB) bonding layer. The III-V active region consists of an n-GaAs bottom contact layer (150 nm thick), an n-$Al_{0.4}Ga_{0.6}As$ bottom cladding layer (70 nm thick), 9 layers of InAs QDs separated by GaAs buffer layers, with a total thickness of 352 nm, a p-type $Al_{0.4}Ga_{0.6}As$ cladding layer (1.5 μm thick) and a p^{++}-GaAs top contact layer (300 nm thick). The confinement factor of the optical mode is 8.9% in the quantum dot layers and 7.5% in the p-AlGaAs layer. The epitaxial layer stack was grown by Innolume [15].

To fabricate the DFB lasers, the InAs/GaAs QD epitaxial structure (10 x 11 mm die) is bonded to the planarized SOI using ultra-thin DVS-BCB adhesive bonding as described in [16]. A DVS-BCB:mesitylene (1:6) solution spin coated at 3000 rpm on the SOI chip and an applied bonding pressure of 100 mbar results in a 60 nm-thick DVS-BCB bonding layer (after curing the DVS-BCB at 250°C). After bonding, the GaAs substrate is removed. For protection of the epi-layers, crystal wax is applied carefully on the edges of the bonded GaAs die such that there is no wax on top of the die that can prevent the etching process. The major part of the GaAs substrate is removed by wet etching in HNO_3:H_2O_2:H_2O. The last 50 μm of the substrate is

Optics EXPRESS

etched using more selective $NH_4OH:H_2O_2$, similar to the process used in [17]. The sacrificial etch stop layers ($Al_{0.85}Ga_{0.15}As/GaAs/Al_{0.85}Ga_{0.15}As$) are then selectively etched using diluted HCl for the $Al_{0.85}Ga_{0.15}As$ layers and citric acid:H_2O_2 for the GaAs layer.

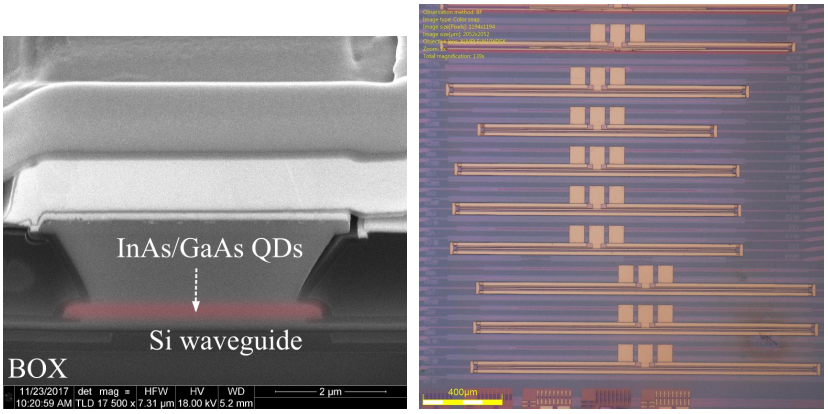

(a) (b)

Fig. 2. III-V/Si distributed feedback laser fabrication: (a) SEM picture of the actual device; (b) Optical micrograph of an array of DFB lasers with GSG contacts.

The III-V mesa and spotsize converter are defined through wet etching, using citric acid:H_2O_2 and KI:I_2:H_2O for the GaAs/InAs and AlGaAs layers, respectively. The reaction rate limited wet etching of the p-AlGaAs cladding layer in KI:I_2:H_2O results in a faceted surface structure dependent on the crystal orientation. Therefore, the lasers should be parallel to the [011] crystal plane of the GaAs wafer. This is illustrated in a scanning electron microscope (SEM) picture of a focused ion beam (FIB) cross-section of the III-V mesa shown in Fig. 2(a). This allows creating undercut structures in the spot-size converter, which relaxes the lithography requirements in the definition of the III-V spotsize converter, which was realized using 300 nm UV contact lithography. Next, the Ni/Ge/Au n-contact was defined through a lift-off process. The devices were passivated using a 300 nm-thick silicon nitride layer deposited by plasma-enhanced chemical vapor deposition (PECVD). The lasers were then planarized with BCB. Thereafter Ti/Au p-contacts were deposited on the p-GaAs contact layer and annealed at 430°C for 30 seconds. Finally vias were formed and probe pad metal was deposited in a ground-signal-ground (GSG) configuration. Figure 2(b) shows a microscope top image of an array of fully processed DFB lasers.

3. Device characterization

Two DFB lasers with grating periods of 392 nm and 400 nm and Bragg wavelengths of 1300 nm and 1320 nm, respectively were investigated. The laser characterization is carried out by coupling the output of the DFB laser to a cleaved standard single mode fiber through a fiber-to-chip grating coupler. The loss of the grating coupler was measured to be around 8 dB. The measurements were carried out with the device on a thermo-electric heater set at temperatures ranging from 20°C to 100°C.

The continuous wave (CW) light-current-voltage (LIV) characteristic of the DFB lasers is shown in Fig. 3, as a function of temperature. Figure 3(b) shows CW lasing is observed up to 100°C for the DFB laser lasing around 1320 nm. We measure output powers up to 2.5 mW in the waveguide at room temperature for both lasers. The ripple observed in the LI characteristics is attributed to parasitic reflections from the grating coupler used for fiber coupling and reflections

Optics EXPRESS

at the taper tip of the III-V material. This could be improved by using low reflection grating couplers [18] and a better taper tip definition. The differential resistance at 70 mA is 4.1 Ω for the 1300 nm laser and 3.6 Ω for the 1320 nm laser.

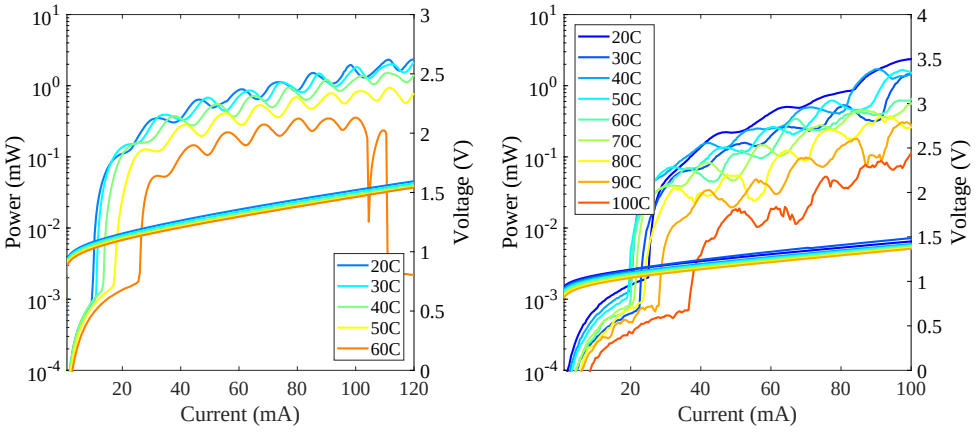

Fig. 3. LIV curve as a function of temperature. The power in the waveguide is plotted. (a) corresponds with the 1300 nm DFB laser, (b) corresponds with the 1320 nm DFB laser.

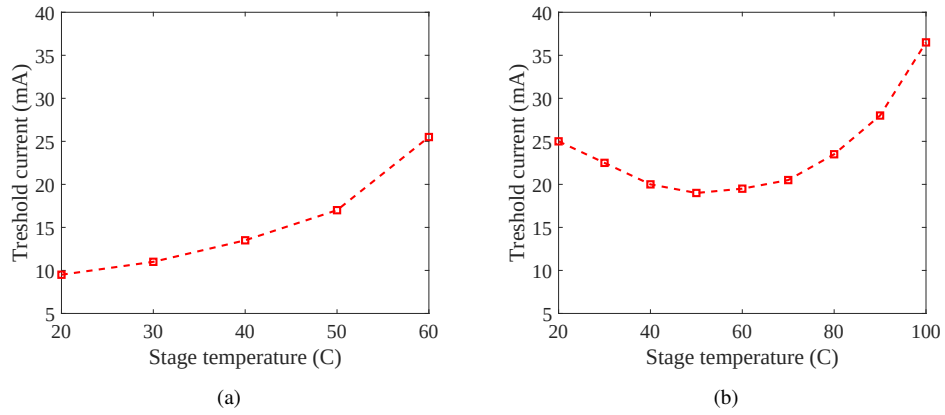

Fig. 4. Threshold current data as a function of stage temperature: (a) for the 1300 nm DFB laser, (b) for the 1320 nm DFB laser

The CW threshold current as a function of stage temperature is shown in Fig. 4. The lowest threshold currents are 9.5 mA, reached at 20°C (shown in Fig. 4(a)) and 19 mA, reached at 50°C (shown in Fig. 4(b)) for the 1300 nm and 1320 nm DFB lasers, respectively. These correspond with a threshold current density of 205 A/cm^2 (mesa width: 3.7 μm and laser length: 1250 μm) and 353 A/cm^2 (mesa width: 3.7 μm and laser length: 1450 μm), respectively. The total coupling strength κL for both devices was estimated by the band gap width to be around 6 for the 1300 nm laser and around 7.7 for the 1320 nm laser. This relatively strong coupling strength results in a low threshold modal gain as described in [19] and thus a low threshold current.

Optics EXPRESS

To understand the behavior of the threshold current as a function of temperature, we have to take into account that in a DFB laser the threshold current depends on the position of the gain peak relatively to the Bragg wavelength, which is determined by the grating period. In the 1320 nm DFB laser, the threshold current decreases with increasing temperature up to 50°C. This is due to the red detuning of the Bragg wavelength with respect to the gain peak at room temperature: when increasing the temperature, the gain shifts to longer wavelengths at a rate approximately ten times faster than the Bragg wavelength and thus aligns better with the Bragg wavelength of the grating. At temperatures above 55°C, the threshold current starts increasing with increasing temperature. In the 1300 nm DFB laser, when increasing the temperature the gain peak shifts away from the Bragg wavelength, resulting in an increasing threshold current. At high temperatures the detuning between the Bragg wavelength and the gain peak becomes that big that it prevents CW lasing above 60°C. To improve the intrinsic temperature stability of the GaAs quantum dot material, the undoped quantum dots could be replaced with p-type modulation-doped quantum dots [20]. Furthermore, all improvements of the thermal sinking, like thicker metal on top and thermal vias will benefit the performance of the laser.

For both DFB lasers, the optical spectrum as a function of temperature for a drive current of 60 mA is plotted in Fig. 5. Laser emission at 20°C is observed around 1298 nm for a grating period of 392 nm, plotted in Fig. 5(a) and around 1322 nm for a grating period of 400 nm, plotted in Fig. 5(b). With increasing temperature the laser output wavelength shifts to longer wavelengths with a temperature coefficient of 0.1nm/°C. We see single mode operation and a side-mode suppression ratio (SMSR) of 47 dB (1298 nm) and 40 dB (1322 nm). The SMSR is not affected by the ripple observed in the LI curve.

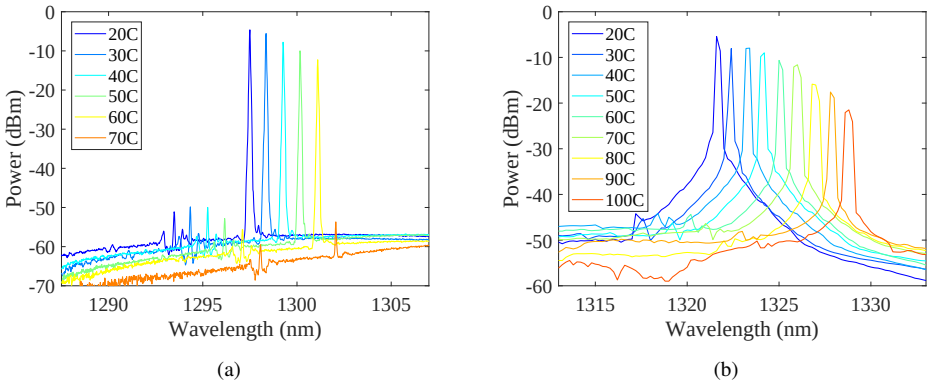

Fig. 5. (a) Optical spectrum for a drive current of 60 mA as a function of temperature: single mode operation with a SMSR of 47 dB. The DFB laser has a grating period of 392 nm. (OSA resolution: 0.06 nm) (b) Optical spectrum for a drive current of 60 mA as a function of temperature: single mode operation with a SMSR of 40 dB for a DFB laser with a grating period of 400 nm. (OSA resolution: 0.1 nm) Note that the difference in shape between the lasing peaks of Fig. (a) and Fig. (b) is due to the fact that different optical spectrum analyzers (OSA) were used to measure both lasers.

Figure 6 shows the optical spectra as a function of drive current at room temperature. At higher drive currents (e.g. from 90 mA at 20°C) higher order modes appear for the 1320 nm DFB laser, as is shown in Fig. 6(b). This is due to lateral higher order modes that exist in the laser mesa as can be seen in Fig. 7. These modes have a similar optical confinement in the active region (8.9% for the fundamental mode and 8.8% for the first order mode) and therefore experience a similar level of gain. They have a slightly lower effective index ($n_{eff,0}$ = 3.31 and $n_{eff,1}$ = 3.29) and thus

Optics EXPRESS

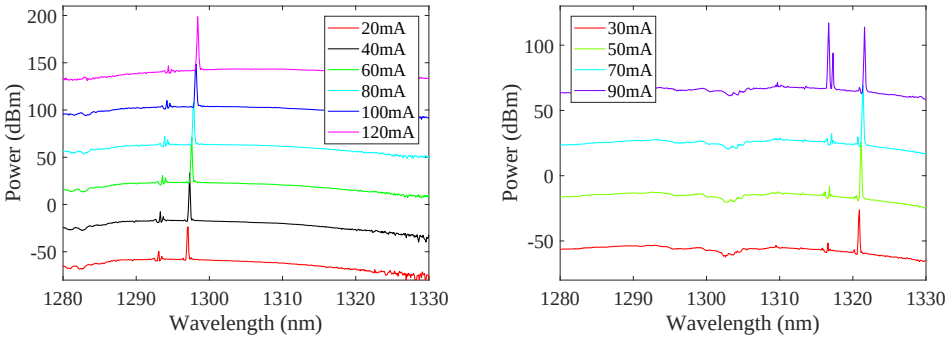

Fig. 6. Optical spectra for different drive currents at room temperature. The different spectra are shifted 40 dB apart for clarity (OSA resolution: 0.06 nm). In (a) the DFB laser has a grating period of 392 nm and in (b) the DFB laser has a grating period of 400 nm.

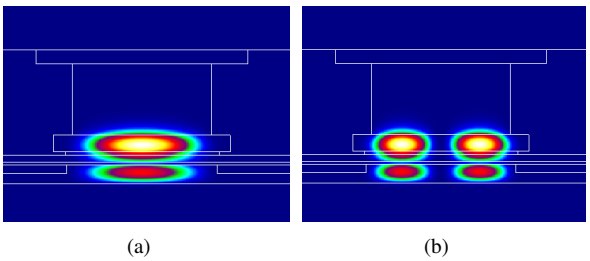

Fig. 7. Mode profiles of the hybrid modes present in the laser cavity: (a) fundamental mode and (b) first order mode.

a lower Bragg wavelength than the fundamental mode ($\lambda_{B,0}$ = 1322 nm and $\lambda_{B,1}$ = 1318 nm). Normally, when an adiabatic taper is present, this taper will act as a mode filter and only the fundamental mode will couple into the silicon waveguide. However, due to imperfect fabrication of the laser mesa the taper tip was too broad, so that the taper was no longer adiabatic. Because of this, the taper became much more sensitive to misalignment compared with a normal adiabatic taper. A small misalignment (300 nm) allowed the first order mode to also couple into the silicon waveguide at higher drive currents in case of the 1320 nm DFB laser. We didn't have the same problem with the 1300 nm laser, since in this case the first order mode is further removed from the gain peak than the fundamental mode and never reaches the lasing threshold.

4. Conclusion

This paper demonstrates a single mode quantum dot DFB laser on a silicon photonic integrated circuit with efficient coupling of light to a silicon waveguide. We demonstrated high temperature operation with CW lasing up to 100°C. Threshold current densities as low as 205 A/cm^2 were measured. The laser showed single mode behavior with a side-mode suppression ratio of 47 dB. The device performance is currently limited by the suboptimal III-V tapers, resulting in residual reflections, extra losses and the existence of higher order modes. We expect significant improvement with better III-V taper structures. These devices are attractive candidates for uncooled transceivers in data centers.

Optics EXPRESS

Acknowledgments

Sarah Uvin thanks the Agency for Innovation by Science and Technology in Flanders (IWT) for a PhD grant.

Disclosures

The authors declare that there are no conflicts of interest related to this article.